Pt Catalysts Prepared via Top-down Electrochemical Approach: Synthesis Methodology and Support Effects

Alexandra Kuriganova[1]*, Igor Leontyev[2], Nikolay Leontyev[3], and Nina Smirnova[1]
[1]*Platov South Russian State Polytechnic University (NPI), Novocherkassk, 346428, Russia*
[2]*Southern Federal University, Rostov-on-Don, 344090, Russia*
[3]*Azov-Black Sea Engineering Institute of Don State Agrarian University, Zernograd, 347740, Russia*

ABSTRACT

The synthesis of Pt nanoparticles and catalytically active materials using the electrochemical top-down approach involves dispersing Pt electrodes in an electrolyte solution containing alkali metal cations and support material powder using an alternating pulsed current. Platinum is dispersed to form particles with a predominant crystallographic orientation of Pt(100) and a particle size of approximately 7.6±1.0 nm. The dispersed platinum particles have an insignificant content of PtO_x phase (0.25±0.03 wt.%). The average formation rate was 9.7±0.5 mg cm^{-2} h^{-1}. The nature of the support (carbon material, metal oxide, carbon-metal oxide hybrid) had almost no effect on the formation rate of the Pt nanoparticles as well as their crystallographic properties. Depending on the nature of the support material, Pt-containing catalytic materials obtained by the electrochemical top-down approach showed good functional performance in fuel cell technologies (Pt/C), catalytic oxidation of CO (Pt/Al_2O_3) and electrochemical oxidation of methanol (Pt/TiO_2-C) and ethanol (Pt/SnO_2-C).

Keywords : Electrochemical synthesis, Pulse electrolysis, Pt nanoparticles, Heterogenous catalysis, Electrocatalysis

Received : 13 February 2024, Accepted : 23 April 2024

1. Introduction

Platinum-based catalysts are commonly used in heterogeneous catalysis, including gas emission neutralisation and fuel cell technology [1]. The catalytic activity of a platinum particle in a particular process is determined by its amount, dispersibility, and structural characteristics. The relationship between metal nanoparticles (NPs) catalytic activity and particle size, known as the “size effect”, is a widely discussed topic. This effect is typically observed in the range of 1–10 nm [2], with catalytic activity decreasing as particle size decreases [3]. On the other hand, the (electro)catalytic activity of platinum-based nanostructures is significantly influenced by the crystallographic planes on which the chemical reaction occurs. For instance, planes (110) and (100) are more active than planes (111) in the oxygen electroreduction reaction and are more resistant to catalytic poisons [4].

The current research and optimization directions for Pt-containing catalysts include (i) developing the optimal composition of the catalytically active phase (binary and multicomponent alloys of platinum with noble and base metals) [5,6], (ii) selecting the optimal support material (carbon materials, metal oxide materials, carbon-metal oxide composites) for the catalytically active phase (metal NPs) [6], and (iii) developing catalysts with different structural characteristics and shapes of Pt particles [7].

Metal NPs can be synthesized using the (electro)chemical bottom-up approach to optimize their performance. In this case, metal NPs synthesis involves electrochemically reducing metal ions to a metallic state. The size of the electrodeposited NPs can be controlled by variation of the electrolysis parameters [8]. However, with this electrochemical bottom-up approach, the metal NPs are only produced on the surface of the working electrode and not on the dispersed support. It should be noted that most industrial applications still require the use of dis-

*E-mail address: kuriganova_@mail.ru

DOI: https://doi.org/10.33961/jecst.2024.00206

persed catalytic systems, where the active catalytic phase is located on the surface of a support material. To obtain such catalytic systems, the impregnation method is the most commonly used approach [9]. The microstructural characteristics of the catalytically active phase (Pt NPs) are greatly influenced by the nature of both reactants (solid surface and liquid) and the reaction conditions. It is important to note that nanoparticles, including platinum, are thermodynamically metastable due to their large surface area [10]. In addition, dispersity stabilisers and capping agents are used during the synthesis process to prevent particle growth and agglomeration. However, these additives may contaminate the final product and negatively impact its catalytic properties. Furthermore, in accordance with the principles of green chemistry, Pt catalysts that are used in environmentally friendly technologies should also be synthesized using environmentally friendly methods. The use of electrochemical techniques in top-down approaches, specifically pulse electrolysis, can be a simple and environmentally-friendly method to disperse Pt electrodes into nanoscale Pt particles: compared to bottom-up electrochemical and liquid-phase chemical approaches for synthesising catalytic materials based on metal nanoparticles, the top-down electrochemical approach does not require the use of organic solvents or stabilisers during synthesis [11]. This paper summarises our study results on the influence of some synthesis parameters (duration, amount and composition of the support) of Pt-containing catalytic systems on their microstructural characteristics during pulse electrolysis synthesis.

2. Experimental

2.1 Synthesis of catalytic materials

The support material was suspended in an electrolyte solution (1 or 2 M NaOH). Concentration of support material in suspension was 3 g L^{-1}. Then

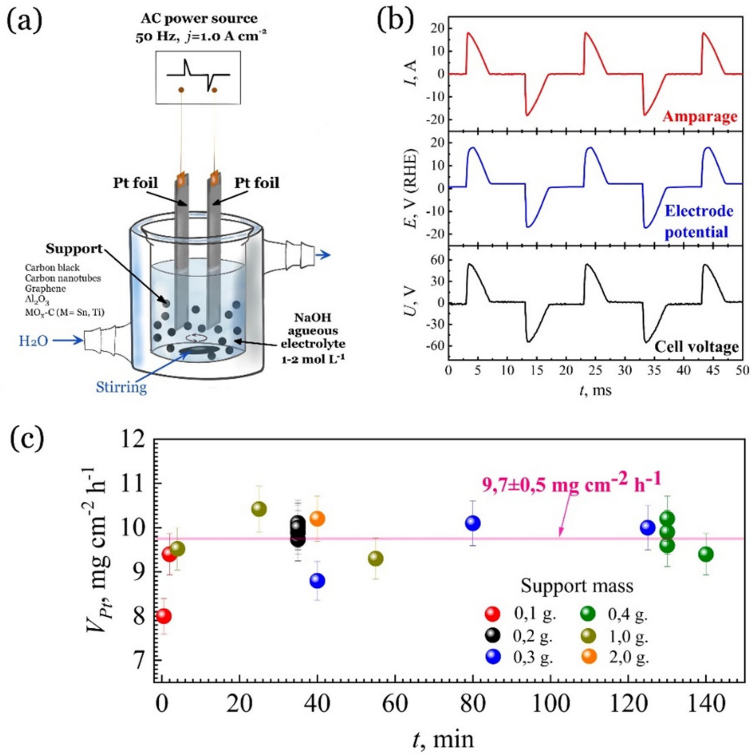

Fig. 1. (a) Schematic representation of experimental set-up of electrochemical preparation of Pt-containing materials under PAC conditions. (b) Profiles of electrical parameters of the electrochemical cell. (c) The rate of formation of Pt electrode dispersion products under pulse electrolysis conditions depends on the synthesis time and the amount of support.

suspension was stirred on a magnetic stirrer (30 min.) in a jacketed cell (Fig. 1a). The support material used included VULCAN® XC72 conductive carbon black; carbon nanotubes obtained by the pyrolysis of propane–butane mixture on Cu–Ni catalyst; the graphene sample was prepared by an electrochemical dispersion of expanded graphite applying an alternating current [12]; γ-Al_2O_3 powder (SASOL SCFa-230); and MO_x-C hybrid supports (MO_x = SnO_2, TiO_2). In the case of hybrid supports, carbon black was added to the alkali solution together with SnO_2 or TiO_2 materials. These materials were prepared using the methods described previously [13,14]. The catalytic material contained 10–60% of SnO_2 and TiO_2.

After that two Pt foil electrodes with the same geometric surface area (6 cm^2 of each electrode) were placed in the suspension of support materials in alkali electrolyte. Pt electrodes were supplied with a pulsed alternating current with an average current density of 1.0 A cm^{-2} and a frequency of 50 Hz. The current profile was characterised by the presence of an anodic pulse and a cathodic pulse (*current-on* period) and pauses after the anodic and cathodic pulses (*current-off* period) (Fig. 1b). Additionally, the PAC software enables monitoring of the potentials of the Pt electrodes during the synthesis using Ag/AgCl reference electrodes and the cell voltage (Fig. 1b). The synthesis was performed with continuous stirring and electrolyte cooling to 40–50°C. After synthesis, the catalyst suspension was filtered and washed with distilled water until the filtrate reached a neutral pH. The catalyst was then air-dried at 80°C until a constant weight was achieved.

The formation rate of Pt electrochemical dispersion products V_{Pt} (mg cm^{-2} h^{-1}) was determined using the following formula:

$$V_{Pt} = \frac{m_{Pt}}{S_{Pt} \times t}$$

where m_{Pt} – mass of dispersed Pt, determined via differences between mass of Pt electrodes before and after synthesis, mg; S_{Pt} – geometric area of Pt electrodes, cm^2; t – duration of the synthesis, hours.

Pt loading in catalytic materials Pt_{theor}, % was determine as follow:

$$Pt_{theor} = \frac{m_{Pt}}{m_{Pt} + m_s}$$

where m_s – mass of support material.

2.2 Physico-chemical analysis

Synchrotron diffraction patterns were recorded at the Swiss–Norwegian Beam Lines (SNBL) at the ESRF (λ = 0.77Å) using a MAR345 image-plate detector. The wavelength, sample-to-detector distance (95 mm), and resolution of the setup were calibrated with LaB_6 powder (NIST). X-ray absorption spectroscopy was carried out using XAS beamline at the ANKA synchrotron radiation source. The catalysts (pressed and sieved to 100–200 μm grains) were placed in in situ microreactors (quartz capillary, 1.5–3 mm diameter, 20 μm wall thickness) heated by a hot air blower (Gas Blower GSB-1300, FMB Oxford). Transmission electron microscopy (TEM) images were obtained with a JEOL EX-1200 unit (30 kV).

2.3 Catalytic tests

The membrane electrode assembly (MEA) of proton exchange membrane fuel cell (PEMFC) measurements were carried out with a single cell (Electrochem®, active geometric area of 1 cm^2). The Pt/C catalyst was directly sprayed onto the Nafion membrane (NRE 212, DuPont, 50 mm thickness) by the pulse-swirl-spray technique, and dried at 60°C in air. The membranes with catalytic layers were connected with two Freudenberg I2C8 gas diffusion layers and annealed by hot pressing at 413 K and 1.0 MPa for 3 min. The Pt loading of the anode and cathode catalysts coating were 0.4 mg cm^{-2} at the humidity of 100% and cell temperature of 25°C.

The electrocatalytic measurements of methanol and ethanol electrooxidation were carried out using standard three-electrode electrochemical cell. Platinum wire was used as a counter electrode. The potentials were measured versus a saturated Ag/AgCl reference electrode. The potentials were related to the reversible hydrogen electrode (RHE). The catalytic ink was prepared with 14 mg of catalyst, 1 mL of isopropanol and 24 μL of a 10 wt.% Nafion solution (Du Pont). The mixture was mixed with a magnetic stirrer (30 min), and 60 μL of the catalytic ink was dropped onto a glassy carbon electrode (the Pt loading of the working electrode was 0.2 mg cm^{-2}) and dried at 80°C in air until a constant weight was achieved. Cyclic voltammograms (CVs) were conducted in a nitrogen-saturated 0.5 M H_2SO_4 contained 0.5 M CH_3OH or 0.5 M C_2H_5OH.

Catalytic tests of Pt/Al_2O_3 materials were carried

out in a fixed-bed quartz flow reactor (inner diameter 8 mm) in a temperature programmed mode while the temperature was cycled between 50 and 250°C (for CO/NO oxidation) at 5°C min^{-1}.

3. Results and Discussion

Applying pulsed alternating current (PAC) to Pt electrodes in strongly alkaline aqueous electrolytes containing alkali metal cations allows for the production of Pt NPs. The mechanism of Pt NPs formation under PAC conditions is due to the intercalation of alkali metal into the Pt crystal lattice, the formation of an intermetallic compound of platinum and alkali metal, and the decomposition of the intermetallic compound by water, resulting in the formation of dispersed Pt. The preparation of Pt NPs under PAC conditions was influenced by the formation of PtO_x phase and their reduction, as well as thermokinetic effects and gas filling of the near-electrode layer. This mechanism has been discussed in detail in [11,15].

During the synthesis process of Pt-containing catalytic systems under PAC conditions, it is important to stir the suspension of support material in electrolyte solution. The support material can be of different natures, such as carbon black, carbon nanotubes, graphene, metal oxide (Al_2O_3), and metal oxide-carbon black hybrid carriers (SnO_2-C, TiO_2-C with dif-

Table 1. Influence of support nature and synthesis time on the formation rate of platinum dispersion products under pulse electrolysis conditions

Sample	Pt loading (wt.%)		Support mass (g)	Synthesis duration (min)	V_{Pt} (mg cm^{-2} h^{-1})	Pt NPs size / characterization method	Ref
	Pt_{theor}[a]	Pt_{obs}					
Pt/Al_2O_3	1.0	0.81[b]	0.1	0.5	8.0	3–4 nm / TEM, CO chemosorption	[16]
	4.0	3.8[b]	0.1	2.0	9.4		
	0.7	0.67[b]	1.0	4.0	9.5		
	10.0	9.4[b]	1.0	55.0	9.3		
	5.0	5.9[b]	1.0	25.0	10.4		
	4.0	4.1[b]	2.0	40.0	10.2		
Pt/Vulcan	20.0	19.9[c]	0.3	40.0	8.8	9.0±1.0 nm / X-ray diffraction	[11,24]
	35.0	35.4[c]	0.3	80.0	10.1	9.0±1.0 nm / X-ray diffraction	
	39.6	38.6[c]	0.4	130.0	9.5	7.6 nm / X-ray diffraction	[19]
	46.0	46.0[c]	0.3	125.0	10.0	9.0±1.0 nm / X-ray diffraction	[24]
	25.0	25.1[c]	0.2	35.0	10.0	10.6 nm / X-ray diffraction	[21]
Pt/CNT	25.0	24.8[c]	0.2	35.0	9.8	7.6 nm / X-ray diffraction	[21]
	40.5	40.0[c]	0.4	130.0	10.2	7.6 nm / X-ray diffraction	[19]
	41.2	40.8[c]	0.4	140.0	9.4	5.6 nm / X-ray diffraction	
Pt/Graphene	25.0	24.8[c]	0.2	35.0	9.8	7.6 nm / X-ray diffraction	[21]
Pt/TiO_2-Vulcan (10% TiO_2)	25.0	-	0.2	35.0	10.0	10.6 nm / X-ray diffraction	[20]
Pt/TiO_2-Vulcan (30% TiO_2)	25.2	-	0.2	35.0	10.0		
Pt/TiO_2-Vulcan (60% TiO_2)	24.0	-	0.2	35.0	9.7		
Pt/SnO_2-Vulcan (10% SnO_2)	25.0	-	0.2	35.0	9.9		
Pt/SnO_2-Vulcan (30% SnO_2)	25.5	-	0.2	35.0	10.1		[17]
Pt/SnO_2-Vulcan (60% SnO_2)	24.8	-	0.2	35.0	10.0		

[a] Determined by the mass loss of the Pt electrodes.
[b] According to X-ray absorption.
[c] According to thermogravimetric analysis.

ferent ratios of MO_x and carbon component). This prevents the agglomeration of formed platinum particles [11,16–24] (Fig. 1a). Simultaneously, the profiles of the primary electrical parameters of the electrochemical cell (Fig. 1b) remained unchanged upon introduction of the support material into the electrolyte solution.

The data analysis (Table 1) shows that the formation rate of Pt electrochemical dispersion products (V_{Pt}) (Fig. 1c) is not significantly affected by the nature of the support under PAC conditions. The average value of the V_{Pt} was 9.7±0.5 mg cm^{-2} h^{-1} for all synthesized Pt-containing materials.

A series of Pt/Al_2O_3 materials (Table 1) characterised by a relatively low platinum content, regardless of the difference in the duration of synthesis, can be observed a sufficient convergence of the results of the determination of the platinum content, both in terms of mass loss of platinum electrodes (Pt_{theor}), and determined by different methods (Pt_{obs}) depending on the type of catalyst support (see footnote in Table 1).

For Pt/C materials (Table 1) with totally different morphology of carbon supports (carbon black and carbon nanotubes), the duration of synthesis as well as the platinum content in the catalyst had no significant effect on the platinum crystallite size determined by X-ray diffraction.

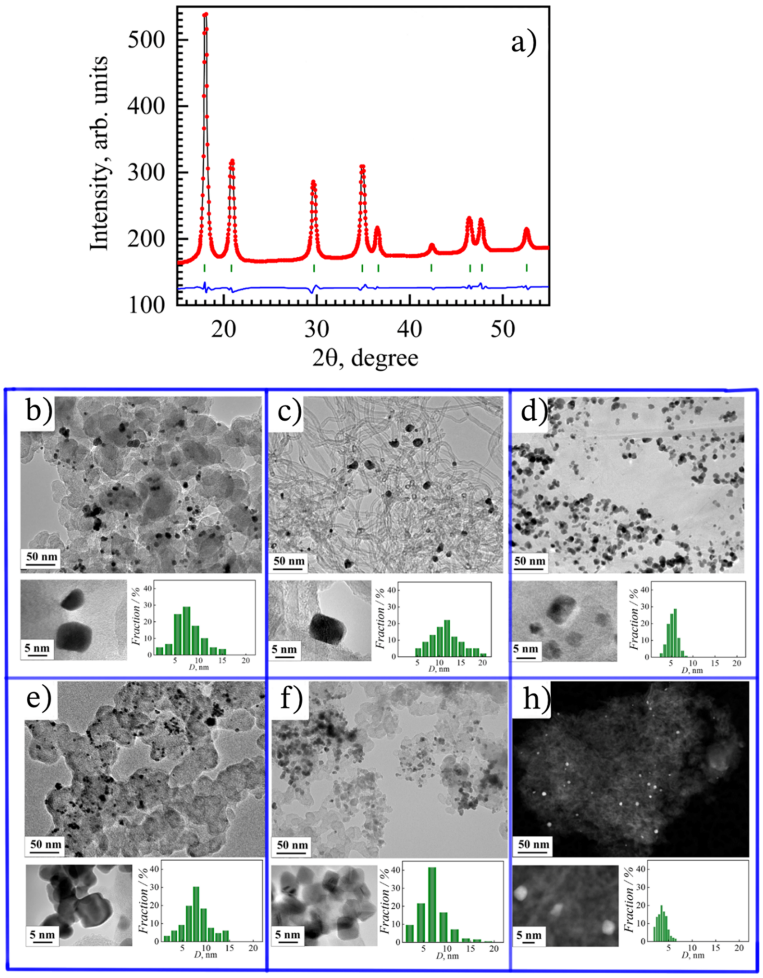

Fig. 2. (a) X-ray diffraction pattern of Pt/Vulcan material (20% Pt) prepared via PAC. Dots: observed intensity, line: intensity calculated by the Rietveld method; blue line: difference between observed and calculated intensities; vertical green bars: positions of Fm3m phase peaks. Inset: TEM image of Pt NPs in Pt/Vulcan material. TEM-images and GSD of (b) Pt/Vulcan, (c) Pt/CNT, (d) Pt/Graphene, (e) Pt/SnO_2-C, (f) Pt/TiO_2-C and (h) HAADF-STEM image of Pt/Al_2O_3.

A series of Pt/MO_x-C materials (Table 1) with different MO_x phase contents and independent of the MO_x phase composition at the same synthesis time demonstrated good convergence of the Pt_{theor} parameter and Pt crystallite size in such materials.

Pt NPs produced via pulsed electrolysis and supported different supports exhibit several unique features.

1) Pt NPs were characterized by the shape of a truncated cube. The results of refining X-ray patterns (Fig. 2a) using the Rietveld method with the spherical harmonics method confirm this [19,25].
2) Pt-based catalysts contain a small amount of PtO_x (0.25 ± 0.03 wt.% Pt) in the form of PtO_2. This was detected by XAS spectroscopy [16] for Pt/Al_2O_3 characterized by relatively low Pt loading. Moreover, the oxidation state of platinum decreased as the platinum content in the Pt/Al_2O_3 material increased.
3) Pt NPs are prone to agglomerate on the support surface. This was confirmed by TEM and grain size distribution (GSD) (Fig. 2b–h). The degree of agglomeration is largely determined by the duration of synthesis, Pt content in the catalyst and nature of support materials.

The varying Pt content intervals in the catalytic systems were a result of the different functional affiliations of the resulting materials. The catalytic prop-

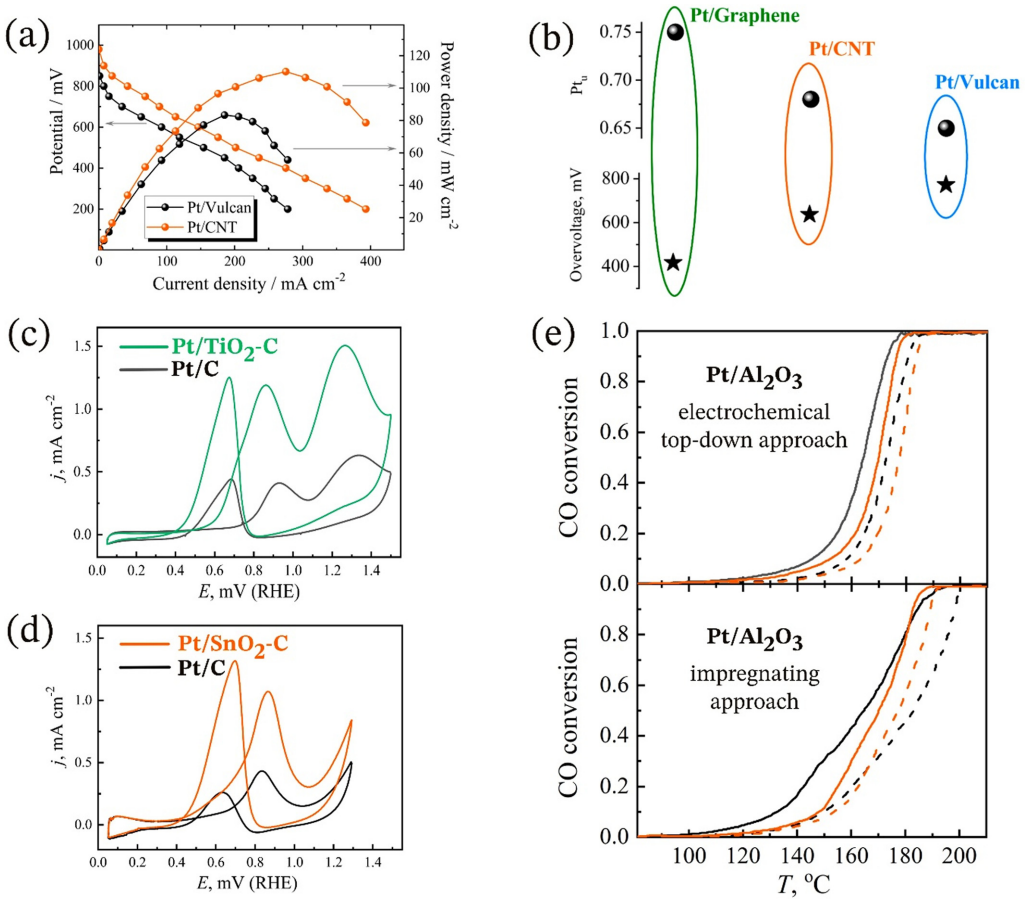

Fig. 3. (a) Voltammetric and power characteristics of air–hydrogen MEA based on Pt/Vulcan and Pt/CNT materials. (b) Dependence of Pt_u parameter and value of overvoltage on support type of Pt/C materials. CV curves of (c) Pt/C and Pt/TiO_2-C catalysts in a 0.5 M CH_3OH + 0.5 M H_2SO_4 solution and (d) Pt/C and Pt/SnO_2-C catalysts in a 0.5 M C_2H_5OH + 0.5 M H_2SO_4 solution acquired at a scan rate of 50 mV s^{-1}. Conversion of CO obtained during CO and NO simultaneous oxidation over Pt/Al_2O_3 catalysts. Solid lines are recorded during heating, dashed lines during cooling. Black curves – as-prepared catalysts, orange curves – aged catalysts.

erties of Pt/Al_2O_3 were studied for selective CO oxidation. Pt/C and Pt/MO_x-C (M= Ti, Sn) materials were studied as electrocatalysts, particularly for fuel cell technology. For instance, carbon black and carbon nanotube catalysts have demonstrated high activity in the MEA of a PEMFC (Fig. 3a) [19]. Graphene as a support material increased Pt utilization (Pt_u) and reduced direct ethanol fuel cell anode overvoltage compared to Pt/CNT and Pt/Vulcan (Fig. 3b) [21]. The electrochemical top-down approach was used to synthesize Pt NPs and a hybrid supports based on metal oxides (TiO_2-C, SnO_2-C). This resulted in materials with enhanced electrocatalytic activity in the electrochemical oxidation reactions of methanol (Fig. 3c) and ethanol (Fig. 3d). The Pt/Al_2O_3 material demonstrated similar catalytic activity in the high-temperature CO oxidation reaction as Pt/Al_2O_3 obtained through the standard impregnation method (Fig. 3e).

4. Conclusions

During pulse electrolysis in an alkaline electrolyte, platinum is dispersed to form particles with a predominant crystallographic orientation of Pt(100) and a particle size of approximately 7.6±1.0 nm. The dispersed platinum particles have an insignificant content of PtO_x phase (0.25±0.03 wt.%). The presence of a carbon (carbon black, carbon nanotubes, graphene), metal oxide (Al_2O_3) or hybrid (SnO_2-C, TiO_2-C) powder support in the electrolyte allows to obtain in a single step deposited electro- and catalytically active Pt-containing materials without the use of capping agents and post-treatment. The duration of synthesis controls the any platinum content in these materials (Pt loading ranging from tenths of a percent up to tens of percent). The crystallographic properties of Pt nanoparticles are independent of the support's nature.

The optimal size and crystallographic orientation of Pt nanoparticles contribute to their high catalytic activity in various oxidative processes, including PEMFCs using Pt/C (based on carbon black, carbon nanotubes, graphene) materials, electro-oxidation of methanol and ethanol using Pt/MO_x-C (M= Ti, Sn) materials, and catalytic CO oxidation using Pt/Al_2O_3 materials.

Acknowledgements

This work was supported by the Ministry of Science and Higher Education of the Russian Federation, project FENN-2024-0002.

References

[1] X. Ren, Q. Lv, L. Liu, B. Liu, Y. Wang, A. Liu, and G. Wu, *Sustainable Energy Fuels*, **2020**, *4*, 15–30.
[2] S. Mukerjee, *J. Appl. Electrochem.*, **1990**, *20*, 537–548.
[3] K. Kinoshita, *J. Electrochem. Soc.*, **1990**, *137*, 845–848.
[4] P. Inkaew, W. Zhou, and C. Korzeniewski, *J. Electroanal. Chem.*, **2008**, *614(1–2)*, 93–100.
[5] G. Yang, Q. Zhang, H. Yu, and F. Peng, *Particuology*, **2021**, *58*, 169–186.
[6] X. Ren, Y. Wang, A. Liu, Z. Zhang, Q. Lv, and B. Liu, *J. Mater. Chem. A*, **2020**, *8*, 24284–24306.
[7] T. Song, F. Gao, S. Guo, Y. Zhang, S. Li, H. You, and Y. Du, *Nanoscale*, **2021**, *13*, 3895–3910.
[8] J. Jang, J. Kim, C. K. Lee, and K. Kwon, *J. Electrochem. Sci. Technol.*, **2023**, *14(1)*, 15–20.
[9] M. J. Ndolomingo, N. Bingwa, and R. Meijboom, *J. Mater. Sci.*, **2020**, *55*, 6195–6241.
[10] R. Ferrando, J. Jellinek, and R. L. Johnston, *Chem. Rev.*, **2008**, *108(3)*, 845–910.
[11] I. Leontyev, A. Kuriganova, Y. Kudryavtsev, B. Dkhil, and N. Smirnova, *Appl. Catal. A General*, **2012**, *431–432*, 120–125.
[12] A. B. Kuriganova, I. N. Leontyev, M. V. Avramenko, N. A. Faddeev, and N. V. Smirnova, *Mendeleev Commun.*, **2022**, *32(3)*, 308–310.
[13] A. B. Kuriganova, C. A. Vlaic, S. Ivanov, D. V. Leontyeva, A. Bund, and N. V. Smirnova, *J. Appl. Electrochem.*, **2016**, *46*, 527–538.
[14] A. Ulyankina, M. Avramenko, D. Kusnetsov, K. Firestein, D. Zhigunov, and N. Smirnova, *Chemistry Select*, **2019**, *4(6)*, 2001–2007.
[15] A. B. Kuriganova, D. V. Leontyeva, and N. V. Smirnova, *Russ. Chem. Bull.*, **2015**, *64*, 2769–2775.
[16] D. E. Doronkin, A. B. Kuriganova, I. N. Leontyev, S. Baier, H. Lichtenberg, N. V. Smirnova, and J.-D. Grunwaldt, *Catal. Lett.*, **2016**, *146*, 452–463.
[17] A. B. Kuriganova, D. V. Leontyeva, S. Ivanov, A. Bund, and N. V. Smirnova, *J. Appl. Electrochem.*, **2016**, *46*, 1245–1260.
[18] A. B. Kuriganova, N. V. Smirnova, I. N. Leontyev, and M. V. Avramenko, *ChemChemTech*, **2019**, *62(9)*, 53–59.
[19] K. Novikova, A. Kuriganova, I. Leontyev, E. Gerasimova, O. Maslova, A. Rakhmatullin, N. Smirnova, and Y. Dobrovolsky, *Electrocatalysis*, **2018**, *9*, 22–30.
[20] A. B. Kuriganova, I. N. Leontyev, A. S. Alexandrin, O. A. Maslova, A. I. Rakhmatullin, and N. V. Smirnova, *Mendeleev Commun.*, **2017**, *27(1)*, 67–69.
[21] A. B. Kuriganova, I. N. Leontyev, O. A. Maslova, and N. V. Smirnova, *Mendeleev Commun.*, **2018**, *28(4)*, 444–446.
[22] A. Kuriganova, N. Faddeev, M. Gorshenkov, D.

Kuznetsov, I. Leontyev, and N. Smirnova, *Processes*, **2020**, *8(8)*, 947.
[23] A. B. Kuriganova and N. V. Smirnova, *Mendeleev Commun.*, **2014**, *24(6)*, 351–352.
[24] I. N. Leontyev, D. V. Leontyeva, A. B. Kuriganova, Y. V. Popov, O. A. Maslova, N. V. Glebova, A. A. Nechitailov, N. K. Zelenina, A. A. Tomasov, L. Hennet, and N. V. Smirnova, *Mendeleev Commun.*, **2015**, *25(6)*, 468–469.
[25] M. Järvinen, *J. Appl. Crystallography*, **1993**, *26(4)*, 525–531.